Half-Fanbeam Collimators Combined with Scanning Point Sources for Simultaneous Emission-Transmission Imaging

Freek J. Beekman, Chris Kamphuis, Brian F. Hutton and Peter P. van Rijk

Department of Nuclear Medicine, Image Sciences Institute, University Hospital Utrecht, Utrecht, The Netherlands; and Department of Medical Physics, Westmead Hospital, Sydney, Australia

One type of SPECT system often used for simultaneous emission-transmission tomography is equipped with parallel-hole collimators, moving line sources (MLS) and electronic windows that move in synchrony with the sources. Although downscatter from the emission distribution is reduced by the use of the electronic window, this still can represent a sizable fraction of the transmitted counts. These systems have relatively poor spatial resolution and use costly transmission sources. **Methods:** Using a two-head SPECT system, with heads at right angles, two ^{153}Gd line sources (5800 MBq each) were replaced by two ^{153}Gd point sources of only 750 MBq each and positioned to move along the focal lines of two half-fanbeam collimators. A suitable acquisition protocol for a moving point source (MPS) system was selected by considering the results of a simulation study. With this protocol, physical phantom experiments were conducted. **Results:** Simulations showed that by using two half-fanbeam collimators, a gantry rotation of 90°, such as used for 180° acquisition with parallel-beam collimators for cardiac imaging, was insufficient. A gantry rotation of 180° resulted in attenuation maps where only an area to the posterior of a 400-mm wide thorax phantom was affected by truncation. The MPS system had a 14.7 times higher sensitivity for transmission counts than the MLS system. Despite the smaller sources in the MPS system, the number of acquired transmission counts was a factor 1.91 times higher compared with the MLS system, resulting in reduced noise. The relative downscatter contribution from ^{99m}Tc (140 keV) in the ^{153}Gd moving electronic window (100 keV) was reduced by a factor of 1.81. Transmission images of a rod phantom with segments containing acrylic rods of different diameters showed an improvement of resolution in favor of the MPS system from about 11 mm to about 6 mm (five instead of two segments of rods were clearly visible). In addition, the noise level in the MPS thorax transmission images was significantly lower. **Conclusion:** The MPS system has important advantages when compared with the MLS system. The use of low-activity point sources is economically beneficial when compared with line sources and reduces radiation exposure to staff and patients.

Key Words: quantitative SPECT; attenuation correction; transmission scanning; fanbeam collimator

J Nucl Med 1998; 39:1996–2003

$\mathbf{P}$hoton attenuation in patients greatly degrades quantitation of SPECT images and introduces image artifacts and distortions. Accurate correction for attenuation can be performed when the density distribution of the patient is known [for example from transmission CT (TCT) images]. Attenuation correction using separate transmission CT is difficult, since the three-dimensional radiograph image needs to be registered accurately to the SPECT scan. Much effort has been expended during the last decade in developing SPECT systems that acquire TCT data simultaneously with the emission data [emission CT (ECT)-TCT scanning]. The use of such systems can improve significantly the diagnostic accuracy of cardiac SPECT for the detection and localization of coronary heart disease (*1*). In addition to attenuation correction, transmission maps can be useful for anatomical localization of activity (e.g., in tumors and infectious foci), for registration of images from other imaging modalities, for dose calculations (*2–4*) and attenuation, map-based, scatter correction (*5–11*). A large variety of hardware configurations and reconstruction algorithms for combined ECT-TCT imaging are summarized in (*12,13*).

One class of ECT-TCT systems uses parallel-hole collimators combined with sheet sources (*14–19*) (Figure 1A). To reduce both radiation dose to the patient and scatter and to improve resolution, the sheet source may be collimated (*14,20*). ECT-TCT systems equipped with parallel-hole collimators have been improved significantly by using high-intensity, moving line sources and an electronic window moving in synchrony with the source ["electronic collimation" (*21*)] (Fig. 1B). The moving electronic window defines a "strip" on the detector in which transmission counts are collected. Counts on the remainder of the detector area are collected into the emission image. In the case of a parallel-hole collimator and a flood source (Fig. 1A), a low number of transmission counts is obtained and a high amount of downscatter from the emission distribution is detected. When the transmission source is a concentrated moving line source, the same amount of transmission counts are acquired in the moving electronic window (Fig. 1B), but the downscatter contribution is lower since downscatter now is acquired only during a fraction of the total acquisition time, as defined by the ratio of the electronic window width to the field size. Therefore, the moving line source (MLS) system permits improved separation of ECT and TCT data and possible use of transmission sources with a lower energy than the radiopharmaceutical, with significantly reduced downscatter, as is shown by the graphs in the bottom row of Figure 1. An MLS system, with two camera heads at right angles, is shown at the left in Figure 2. An advantage of parallel-hole geometries, compared with most converging geometries, is that truncation of the subject in projection images is avoided in nearly all cases provided the camera field size is sufficiently large. The disadvantage is that the required activity of a fresh ^{153}Gd line source is relatively high (typically 100–250 mCi). Even with this source activity, very few TCT counts are acquired in some pixels when large patients are scanned. This leads to problems in reconstruction, especially when these low-count pixels have to be corrected for downscatter from ^{99m}Tc. Regular replacement of ^{153}Gd line sources (half-life 241.6 days) is expensive, and difficulties have been experienced by some departments in obtaining licenses for the use of these potent sources. The degrading effects of downscatter can be corrected (*21,22*), albeit at the cost of some noise amplification. This noise

FIGURE 1. Comparison of ECT-TCT geometries: (Top row) diagram of the system; (bottom row) indication of relative number of acquired ^{153}Gd transmission counts (T) compared with the emission downscatter counts from ^{99m}Tc (E_d) detected in ^{153}Gd window at 100 keV and at position on the detector where transmission radiation has traversed large attenuating object. Relative height of bars is based on approximations. (A) Parallel-hole collimator and transmission flood source. (B) Parallel-hole with moving line sources. (C) Fanbeam with fixed line source. (D) Fanbeam with moving point source.
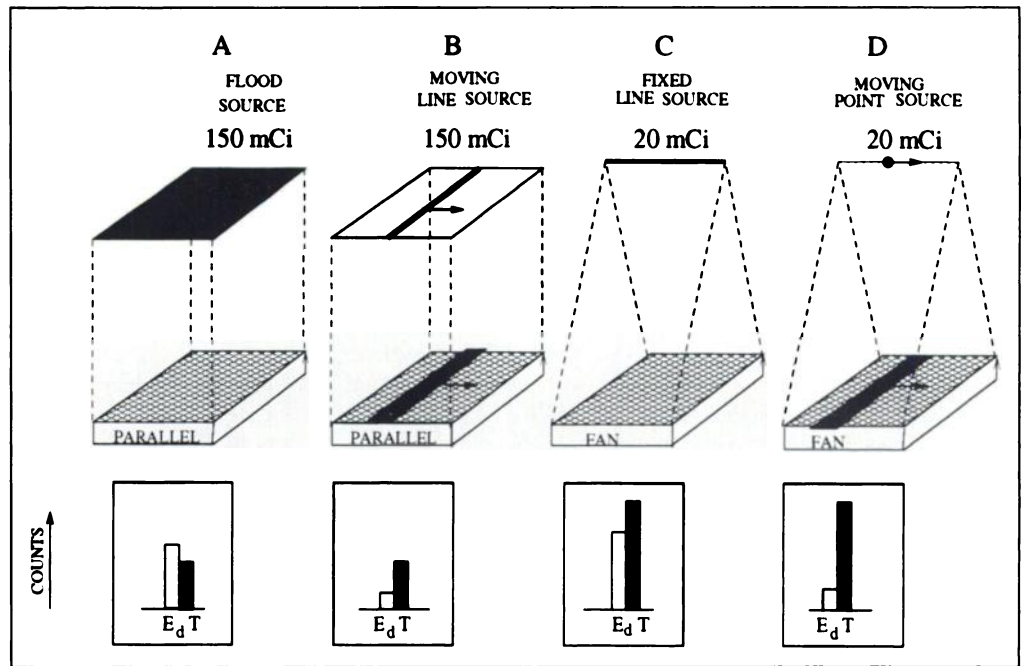
amplification is lower when the relative amount of downscatter is lower. The resolution of TCT images produced by parallel geometries is poor compared with ECT-TCT systems equipped with converging beam geometries (23). Despite these drawbacks and the additional costs for the electronic and mechanical devices to translate the source, scanning line source systems are currently available from several manufacturers.

Another class of methods for ECT-TCT uses fanbeam collimation with a transmission line source in the focal line (Fig. 1C) (23–27). The resolution of fanbeam TCT images is much higher than parallel-beam TCT images (23) since the measurements approximate line integrals originating from a small-diameter source. The activity of the line source is substantially lower than that needed for parallel geometries and is limited by the counting rate of the gamma camera (26). However, projection images of large patients often are truncated for a substantial number of angles. This causes undersampling and, therefore, artifacts in the outer region of the field of view (Fig. 5, top right). Although efforts have been made to reduce the effects of truncation (for example, by including some form of support in the reconstruction), truncation potentially leads to artifacts in the final reconstruction. Consequently, truncation should be minimized, for example, by using asymmetric fanbeam colli-

mators (12,27–33). As with the parallel-hole geometries, contamination of transmission data by downscatter is substantial in the case of simultaneous ECT-TCT acquisition with fanbeam collimators (34). Correction for this photon crosstalk is possible at the cost of increased noise in the transmission image.

To further improve sensitivity and resolution of both emission and transmission imaging, cone-beam collimators can be used (35). However, the problem of truncation in cone-beam tomography is even worse than in fanbeam reconstruction and, therefore, these geometries may be insufficient for ECT-TCT imaging of large objects with currently available detector sizes.

The aim of this study was to develop an ECT-TCT geometry that is optimal for acquiring cardiac images. A dual-head SPECT system was equipped with half-fanbeam collimators and point sources that moved along the lines of focus of the half-fanbeam collimators (Fig. 2, right). In this way, the advantages of fanbeam collimation (high resolution, high sensitivity) and a moving source plus moving electronic window (to reduce relative downscatter) were combined (Fig. 1D). The required acquisition for adequate sampling of a cardiac study, transmission and emission image quality and sensitivity of the system for both downscatter and emission counts from the cardiac region were investigated.

FIGURE 2. System with two heads at right angles for simultaneous ECT-TCT imaging with moving sources and moving electronic windows. (Left) System with parallel-hole geometry and moving line sources (MLS). (Right) System with half fanbeam collimators and moving point sources (MPS). Sources move in axial direction and are collimated in axial direction to only irradiate strips defined by moving electronic windows.
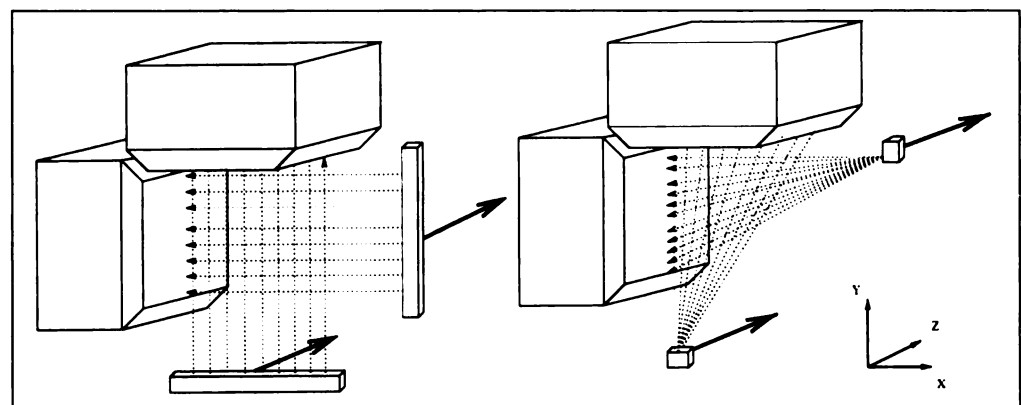
MATERIALS AND METHODS

### Point Source Moving Along Focal Line of Asymmetric Fanbeam Collimator

In Figure 2, two different SPECT geometries with moving sources and moving energy windows are shown. In both the sources are collimated in the axial direction to irradiate only the moving electronic window. At the left is an MLS system equipped with two parallel-hole collimators (hole length 54 mm, hexagonal hole diameter 2.03 mm, septum thickness 0.152 mm) and two ^{153}Gd moving line sources of 5800 MBq (156 mCi), diameter 1.5 ± 0.1 mm, length 508 ± 3 mm. This attenuation-correction system (Vantage®, mounted on an ADAC Vertex SPECT system; Milpitas, CA) was used for comparison with the moving point source (MPS) system mounted on the same SPECT camera.

The MPS system used two asymmetric fanbeam collimators and two moving ^{153}Gd point sources (Fig. 2, right). The collimators were manufactured by the lead casting method (Nuclear Fields BV; Vortum Mullem, The Netherlands). The hole length of the fanbeam collimator was 51 mm, the diameter of the hexagonal holes was 1.90 mm and the septum thickness was 0.23 mm. The distance from the crystal to the focal line was 890 mm, and the focal offsets were 257 mm and −257 mm resulting in two half-fanbeam collimators with opposed offsets (Fig. 2, right frame). This permits positioning the patient close to the detectors and minimizes truncation artifacts on the anterior and left lateral sides of the patient.

Since all collimator holes in the central slice of the moving electronic window pointed to the concentrated point source, a greatly increased sensitivity for transmission data was obtained with a limited amount of activity, rather than by a parallel collimator receiving transmission data from a strong line source. The current choice of point-source activity of 750 MBq (20.3 mCi) for each source resulted in a 1.91 times higher number of transmission counts in the blank scans compared with the use of line sources (with activity as stated above). Accounting for relative activities, the sensitivity for transmission counts was a factor 14.7 times higher than for an MLS system. The dimensions of the point sources were: diameter 1.5 ± 0.1 mm, length 3.0 ± 0.5 mm. The choice of the point-source activity was limited by the dead time of the cameras. Using the current activity, the counting rate during acquisition of blank scans was 52 Kcts per sec, with no need for dead-time correction.

Both the line source and the point source used a source holder that was supplied with the ADAC Vantage attenuation-correction system. The source holders contained a rotating lead shutter (diameter 14.1 mm, distance between shutter halves 3.2 mm) and a slit (width 1 mm) for axial collimation (Fig. 3). The slit-to-source distance was 48 mm. The position of the shutter in the point source and the line source was identical, resulting in approximately the same axial width of the irradiation pattern on the moving electronic window. The width of the electronic window was 13% ($\approx$ 49 mm) of the total axial width of the detector (380 mm).

Both the line and point sources were translated by a mechanical device provided by the camera manufacturer (ADAC Vantage attenuation-correction system). This device included a rotating spindle that transported the line-source holder. Poor reproducibility of the source speed can cause nonuniformities in the axial direction, which can differ for different projections. To check whether this was the case, 20 blank scans were acquired under different gantry angles, and 52-pixel wide (254.44-mm) line profiles, drawn perpendicular to the transportation direction of the line source, were analyzed for reproducibility. The average standard deviation in the profile bin values was 46.29 [2.19% of the average counts in the profile bins (2113.6)]. The standard deviation blank scan pixels
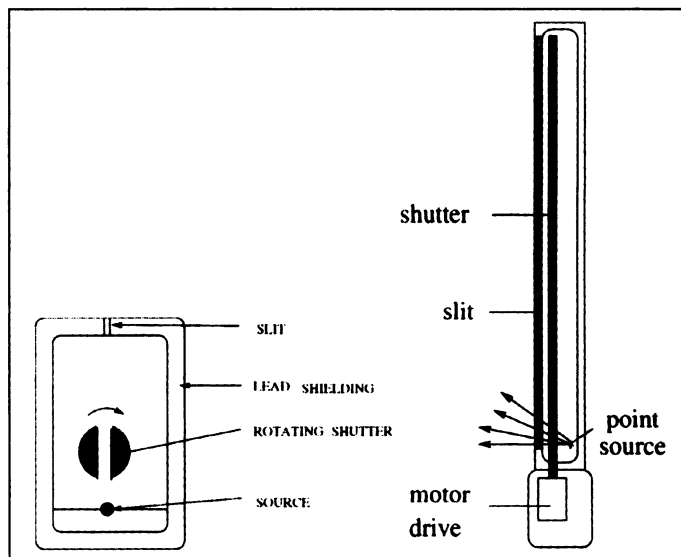
FIGURE 3. Line and point-source holder. (Left) Cross-section of source holder. (Right) Source holder with point source. Point source can be replaced by line source.

(based on 40 counts in a 4.72 mm × 4.72 mm pixel), caused by Poisson statistics only, was 15.8%. This means that the standard deviation caused by mechanical inaccuracies in individual pixels was small compared with the other sources of error. The results in this article were based on this quality of blank scans.

Reconstruction Algorithms

Transmission images of both MLS and MPS geometries were reconstructed with an iterative algorithm [convex algorithm, (36)]. The number of iterations performed was 45, and a uniform start image was used. A projector backprojector that incorporates a transformation that accounts for the half-fanbeam geometry (37) was implemented.

The emission images were reconstructed by the maximum likelihood expectation maximization (ML-EM) algorithm as formulated in Lange and Carson (38). Sixteen iterations of the ML-EM were performed. The projector backprojector incorporated the same fanbeam transformation as was used for reconstruction of the transmission map. Depth-dependent resolution and scatter were not included. Only nonuniform attenuation and varying sensitivity for emission radiation due to the varying collimator hole angle of the fanbeam collimator were modeled in the reconstruction algorithm. The method that accounts for varying collimator hole angle is clarified in Figure 4. Modeling of the varying sensitivity over the field of the fanbeam collimator in the emission reconstruction was accomplished by taking into account the fact that the number of holes per pixel and, thus, the sensitivity for emission counts, is reduced when the angle α of the collimator holes increases. If constant hole length is assumed, the sensitivity is proportional to $\cos \alpha$. The constant hole length was achieved by reducing the collimator thickness with increasing offset x (Fig. 4).

Simulation to Assess Acquisition Geometry

With parallel-beam collimators, an acquisition angle of 180° is known to be sufficient to sample the entire object. For a system with two heads at right angles, this means that the gantry has to rotate only 90°. For a single, symmetrical, fanbeam collimator, it is sufficient to acquire over 180° plus the fan angle. The MPS geometry differs in that the fanbeam collimators are asymmetrical and have opposed offsets similar to that shown in (12). Therefore, the effect of acquiring TCT projections with different gantry rotation angles was investigated. Simulation of the transmission data was performed with a projector that calculated the attenuation
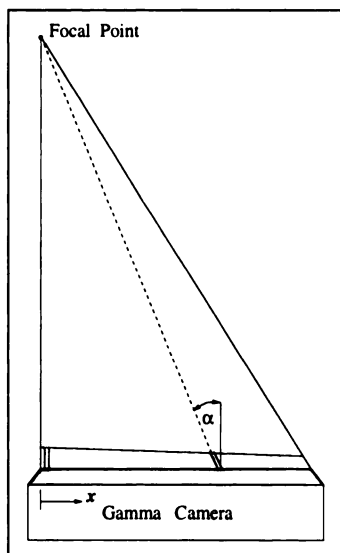
FIGURE 4. Due to increasing hole angle with increasing x, reduced number of holes per bin collect photons. Hole length is kept constant over field of view by reducing collimator thickness with increasing x.

paths through the object. The focal line locations were equal to those in the real system. The acquisition angle and geometry (focal distance and offset) were modeled by transforming the attenuation distribution [similar to Zeng et al. (37)]. The beginning and ending positions of the gantry in the MPS system are shown in the bottom row of Figure 5. The attenuation distribution (Fig. 5, top left) was based on the digital MCAT thorax phantom (39). The phantom was 400 mm wide. The simulations were performed on a relatively fine grid (128 × 128 pixels) compared with the reconstruction of the simulated projections (64 × 64 pixels) so as to partly simulate the continuous character of real data. Since the simulation study was performed to verify completeness of sampling, no noise was added. The simulated transmission images were assessed by visual inspection (Fig. 5).

Physical Phantom Experiments

Rod Phantom Transmission Images. To compare the resolution of transmission maps of MLS and MPS systems, a rod phantom insert (Model ECT/STD/P; Data Spectrum Corporation, Hillsbor-

ough, NC) was used. The diameters of the acrylic rods in the six pie-shaped sectors were 4.8, 6.4, 7.9, 9.5, 11.1 and 12.7 mm. The center-to-center distance of the rods was twice the diameter of the rods.

Based on the results of our experiments described earlier, the fanbeam projection data were acquired for 120 projections during 180° gantry rotation with start and stopping positions as shown at the right in the bottom row of Figure 5. The projection pixel size was 4.72 mm, the matrix size was 128 × 128 and the time per projection was 25 sec. Over this time, the source was translated along the entire detector (380 mm wide). The parallel data were acquired over 180° (90° gantry rotation) with acquisition angles as shown at the left in the bottom row of Figure 5.

Anthropomorphic Thorax Phantom

To test the MPS system under circumstances that were close to those in cardiac studies, a nonuniform thorax phantom (size 380 × 260 mm; Model ECT/TOR/P; Data Spectrum Corporation) was imaged. The thorax phantom contained lungs filled with a mixture of styrofoam and water ($\approx$ 1/3 water density), a liver, a Teflon spine and a heart insert. The same acquisition parameters as for the rod phantom were used, except that 60 projections were acquired.

To evaluate the emission images and effects of downscatter on the transmission images, the thorax phantom was filled with ^{99m}Tc. The amount of activity in the left ventricle wall was 18 MBq ($\approx$0.15 MBq/ml), the background contained 68 MBq ($\approx$ 0.0075 MBq/ml), the liver contained 84 MBq ($\approx$ 0.07 MBq/ml) and the lungs contained 13.7 MBq (left) and 16.2 MBq (right) ($\approx$ 0.015 MBq/ml). The amounts of activity were based on values found in (40) and were derived from ^{99m}Tc-sestamibi cardiac studies. The emission acquisition time was 25 sec per view. The transmission acquisition time was 24 sec per view.

The amount of downscatter can be important in the case of low transmission counts; therefore, the downscatter was, compared with the total transmission counts. The global downscatter fraction was defined as the total number of downscatter counts in all projections, divided by the total number of transmission counts in all projections when no attenuating object was present. The total
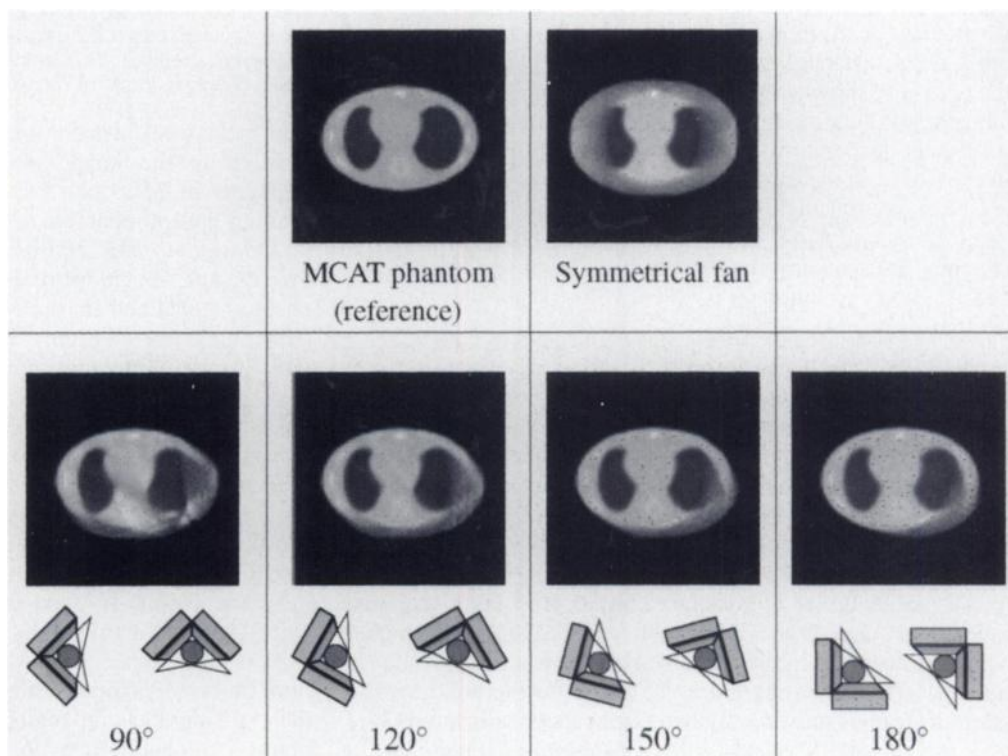
FIGURE 5. Simulation study for assessment of transmission maps at different gantry rotation angles. (Top left) Slice of density distribution of MCAT thorax phantom. (Top right) Reconstructed attenuation map based on 400-mm wide detectors with symmetrical fanbeams, with 500-mm focal distance (41). (Second row) Images based on simulated acquisition with double-headed system (detector width 510 mm) and half fanbeam collimators (Fig. 2). Gantry rotation angles equal 90°, 120°, 150° and 180°. Beginning and ending positions of clockwise gantry rotation are shown in bottom row.
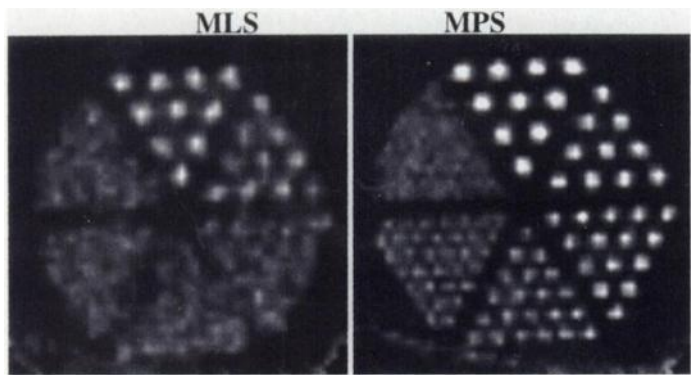
FIGURE 6. Transmission scan of rod phantom. (Left) Slice of rod phantom reconstructed from parallel-hole data. (Right) Reconstruction based on data acquired by half-fanbeam collimators and moving point sources. In both cases, total acquisition time was 12.5 min.

amount of downscatter in the projections was measured by closing the shutter during acquisition of a thorax phantom filled with activity.

For MPS systems, the sensitivity increased because fanbeam collimators were used. On the other hand, the fraction of counts originating from the heart decreased because, for a 180° gantry rotation, in some views from the back, more attenuating tissue was present between the heart and the detector. To compare the sensitivity of the MLS system and MPS system for counts emitted from the heart, measurements with the anthropomorphic thorax phantom with 21.6 MBq in the left ventricle wall were performed. In this experiment, no activity was present in the other segments of the thorax. The total acquisition time for MLS and MPS was equal. The gantry rotation for MLS was 90° and for MPS 180°, as in the measurements described earlier.

RESULTS

Simulation to Assess Acquisition Geometry

In Figure 5 reconstructions based on 120 projections acquired over different gantry rotation angles are shown. For reference, in the top row, the true density distribution (slice of the digital MCAT phantom) and a reconstruction of a simulated transmission map of a triple-head system with a fanbeam collimator with a focal distance of 500 mm and a detector width of 400 mm *(41)* are shown. For the double-head system with half-fanbeam collimators, a single gantry rotation of 90° was insufficient (second row, left); the attenuation factors were affected, even in the cardiac region. The results improved when the gantry rotation angle was increased (second, third and fourth from left, second row). The beginning and ending positions of the gantry are shown in the bottom row. Based on these results, a 180° gantry rotation was chosen for acquiring physical phantom data.

Physical Phantom Experiments

Rod Phantom Transmission Images. In Figure 6 transmission images of the rod phantom are shown. The data were acquired by MLS and MPS with equal acquisition times. Both images were noisy since a small slice thickness (9.44 mm) was used. Better images for both geometries can be obtained by summing a larger number of slices and/or using longer acquisition times. The current choice, however, was closer to the slice thickness typically used under clinical circumstances. It is clear from Figure 6 that use of the MPS system resulted in a much higher resolution than that of the MLS system. Rods in five of the six segments (smallest rods 6.4 mm) were visible in the MPS system instead of rods in only two segments (smallest rods 11.1 mm) for the MLS system. The resolution of parallel- or
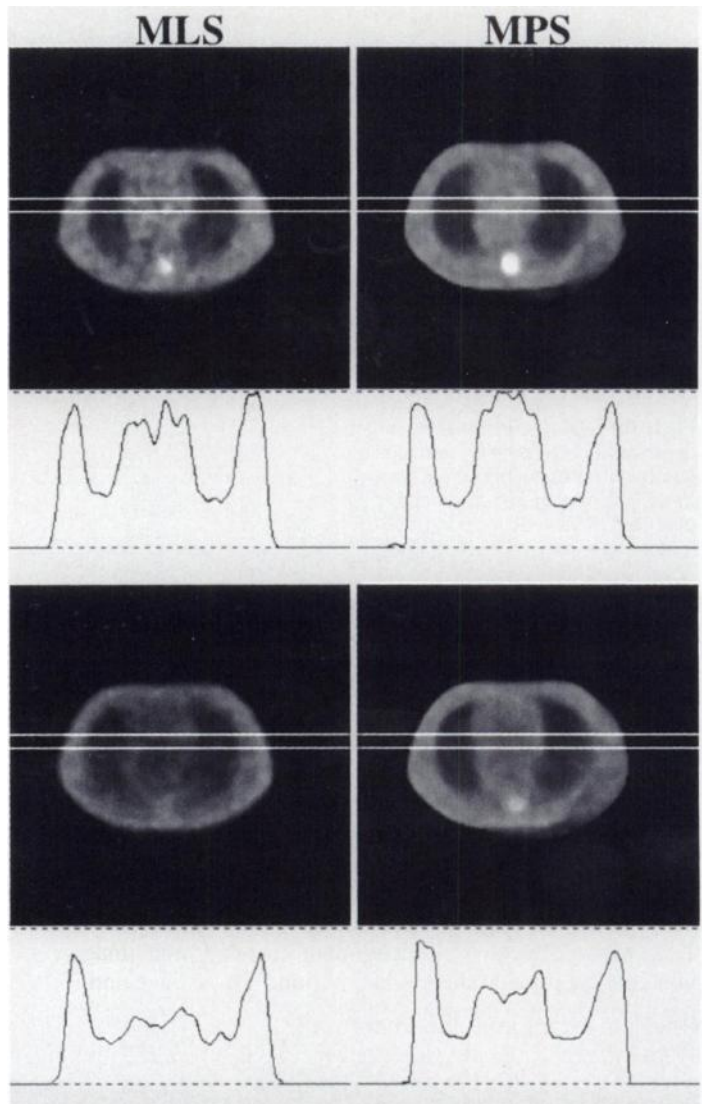
FIGURE 7. (Left) Slices with image profiles of transmission images of thorax phantom reconstructed from parallel-hole data (90° gantry rotation). (Right) Reconstruction based on data acquired by half-fanbeam collimators and moving point sources (180° gantry rotation). (Top) Without emission activity in thorax phantom. (Bottom) Thorax phantom containing activity.

slant-hole transmission images varies significantly with the position in the image plane *(42)*. The number of visible segments in MLS can be varied between one and three by rotating the rod phantom.

Anthropomorphic Thorax Phantom. In Figure 7 transmission images and image profiles of the anthropomorphic thorax phantom, obtained by the MLS and MPS systems, are shown (slice thickness 9.44 mm). To reduce noise but preserve edges, both images were postprocessed twice by applying a three-dimensional median filter with a window length of 3 pixels. The mean and standard deviation of the density were measured in a rectangular region (10 × 10 pixels) in the cardiac (central) area of the thorax phantom. For the phantom without activity (Fig. 7, top row), the mean and standard deviation for MLS were 0.911 and 0.118, respectively, and for MPS 0.983 and 0.071, respectively. For the phantom with activity (Fig. 7, bottom row), these numbers were 0.477 and 0.065 (MLS) and 0.677 and 0.044 (MPS). Thus, a significantly lower bias and noise were found in MPS. Furthermore, the MPS images showed improved resolution. In the MPS image, effects of truncation were seen only on the right dorsolateral region of the transmission image. This region is probably of minor importance for attenuation correc-
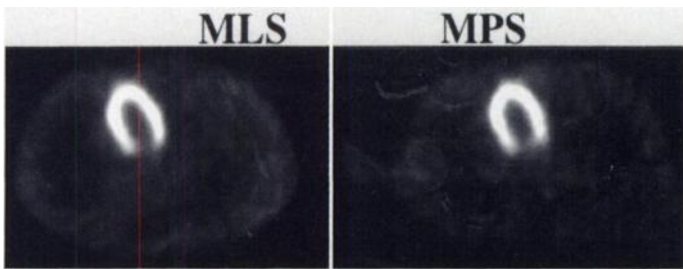
FIGURE 8. Transaxial slices of ^{99m}Tc emission images of thorax phantom reconstructed from parallel-hole data with 90° gantry rotation (left) and from half-fanbeam collimators and moving point sources with 180° gantry rotation (right).

tion (*43*). The truncation effects appeared to agree with those seen in the images of the simulation study. The noise level of the images of the phantom containing activity was lower than for the empty phantom. This was caused by the increased count level in the transmission window when downscattered photons were collected. The downscatter introduced a substantial bias in the transmission maps.

The total blank scan counts for parallel-hole and fanbeam acquisitions were 30912 and 59043 Kcts, respectively; the amount of downscatter was 428 Kcts and 449 Kcts, respectively. Thus, a 1.81 times lower global downscatter fraction was measured for MPS than for MLS. This explains why the parallel-hole images were affected more by downscatter than the fanbeam images.

In Figures 8, 9 and 10, emission images of the thorax phantom and reoriented slices through the left ventricle insert are shown. To reduce noise, the emission images were postfiltered with a three-dimensional Gaussian filter with a FWHM of 1.6 pixels. Effects of truncation of the emission images are visible only outside the cardiac region. The images and image profiles in Figures 9 and 10 show very similar results for both systems.

The acquired number of emission counts from the heart in the half-fanbeam collimators was 9.7% higher than in the parallel-hole collimation. The lead septa used for the fanbeam collimator was thicker than for the parallel-hole collimator. If the same septal thickness had been chosen for the parallel collimator, its counting rate would have decreased by 7.3%. This means that the potential increase in sensitivity by using the half-fanbeams and 180° gantry rotation could be as high as 18%, in compar-
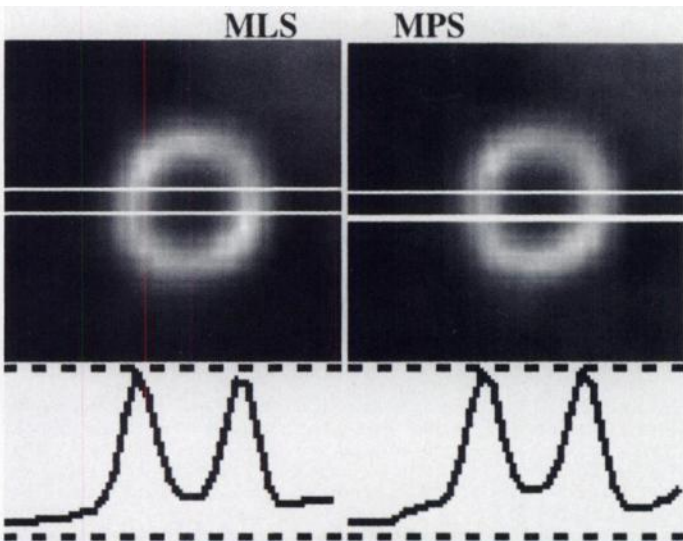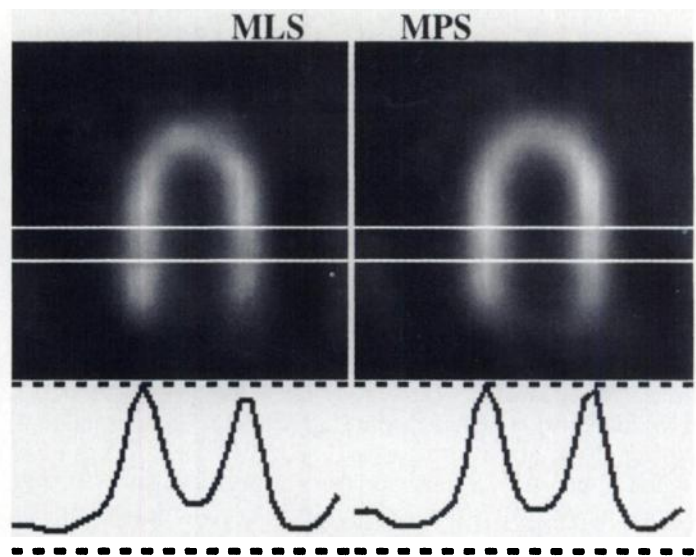
FIGURE 10. Slice of vertical, long-axis image.

ison with the choice of parallel-beam collimators and a 90° gantry rotation.

DISCUSSION

It has been demonstrated that an MPS system has advantages when compared with moving line sources, in terms of noise and spatial resolution of the transmission map, sensitivity for emission counts from the heart and relative downscatter contamination of transmission data. Furthermore, lower activity transmission sources are sufficient. Our results were obtained with point sources with 7.6 times lower activity than the line sources tested. Low-activity sources have advantages in terms of cost and radiation exposure to patients and staff and use of a lower activity may obviate the need for a special radiation license for the use of TCT systems. In addition the MPS system allowed use of lower weight source holders, thus aiding mechanical transportation during scanning.

The resolution of transmission images obtained by MPS was much higher than for MLS. It has been shown that poor resolution may be a possible cause of hot spots in the posterior left ventricular heart wall in attenuation-corrected images (*44*). Also, for other applications, such as scatter compensation, image registration, visualization and volume estimation and availability of high-resolution attenuation maps may be important. Several groups have shown that accurate modeling of scatter is important for obtaining highly quantitative images (*6,9–11,45,46*) and progress has been made in improving practical scatter models, which are a function of the attenuation map (*10,47*). We believe that the quantitative accuracy and resolution of attenuation maps will be important or optimal reconstruction with such models. The resolution of MPS transmission images in the current study was limited by the pixel size available for acquisition. To further improve the resolution, reduce noise and reduce the downscatter contamination, it may be possible to use more active and, perhaps, smaller point sources. Depending on the camera system, however, this may introduce counting rate problems. The use of an attenuating wedge in front of the source requires higher source activity and leads to improved dynamic range (*27*). Optimization of the size and activity of the point source is a subject of further investigation.

A potential disadvantage of the MPS system with 180° gantry rotation in comparison with the MLS system is the truncation of

FIGURE 9. Slice of short-axis image.

large objects. However, a recent simulation study (43) showed no significant differences between attenuation-corrected emission images based on truncated and untruncated transmission data, even for cases with extremely strong truncation. The reason for the small difference may be that the truncation was only present on the reverse side of the object and, therefore, only affected the calculation of attenuation for a few views. Note also that a similar study (40), for three-head ECT-TCT systems with a long focal distance, indicates that truncation does not have a significant effect on attenuation correction. In such systems, a large number of projections are truncated.

Despite the extremely small difference in reconstructed emission images, physicians may feel uncomfortable with truncated attenuation maps. Possible methods of reducing truncation effects include: (a) extrapolation of the transmission projections (48); (b) using a larger focal distance; (c) using a tighter support to reconstruct the attenuation map (49); (d) increasing the acquisition arc; and (e) using an orbit that aligns the camera head as closely as possible to the patient contour. For a single half-fanbeam and a 360° orbit, it has been shown that excellent truncation-free maps can be acquired (27). However, a gantry rotation angle larger than 180° has the disadvantage that the heart may lie outside the collimator's field of view in several projections and, thus, reduced counts are acquired from this organ. A smaller gantry rotation angle permits acquisition of more counts of the heart region but results in stronger truncation of the attenuation maps. It may be possible that a different number of projections or a slightly different start and stop acquisition angle may result in improved cardiac images. Optimizing of the focal distances, offsets and the associated sampling for cardiac imaging, as well as for other imaging procedures, are subjects of further investigation.

In addition to the application outlined in this article, the use of scanning point sources has a potential application for attenuation correction in coincidence imaging, for example, on systems with two opposed camera heads. The function of the collimator in SPECT is twofold for ECT-TCT. First, the emission photons need to be collimated to determine the location of the emission sources. Second, the collimator acts as a scatter grid for transmission photons and reduces emission counts in the transmission window. In coincidence imaging no physical collimation is needed and, therefore, the emission counts are collected more efficiently. Reduction of scatter and emission counts in the transmission window, which is especially required when a point source of lower energy than the emission energy is used, can be achieved by using only a narrow strip of fanbeam collimator, moving in synchrony with the electronic window and the point source, rather than a fanbeam collimator covering the entire detector.

CONCLUSION

A system with moving point sources and half-fanbeam collimators is proposed for simultaneous emission and transmission imaging. The MPS system was implemented on a SPECT system, with the camera heads at right angles, and with moving electronic windows that track the location of the transmission events.

The MPS system provides improved resolution compared to the MLS system but also has markedly better sensitivity, permitting use of lower activity sources. Also the higher sensitivity reduces the influence of emission downscatter. Although some truncation effects were observed in the dorsolateral wall of the object, these did not appear to influence the accuracy of emission reconstruction (43). The MPS system,

therefore, is appealing for simultaneous emission-transmission tomography.

REFERENCES

1. Ficaro EP, Fessler JA, Shreve PD, Kritzman JN, Rose PA, Corbett JR. Simultaneous transmission/emission myocardial perfusion tomography. Diagnostic accuracy of attenuation-corrected ^{99m}Tc-sestamibi single-photon emission computed tomography. Circulation 1996;93:463–473.
2. Zanzonico PB, Bigler RE, Sgouros G, Strauss A. Quantitative SPECT in radiation dosimetry. Semin Nucl Med 1989;19:47–61.
3. Sgouros G, Barest G, Thekkumthala G, Chui C, Mohan R, Bigler RE, Zanzonico PB. Treatment planning for internal radionuclide therapy: Three-dimensional dosimetry for nonuniformly distributed radionuclides. J Nucl Med 1990;31:1884–1891.
4. Giap HB, Macey DJ, Podoloff DA. SPECT-based three-dimensional treatment planning system for radioimmunotherapy. J Nucl Med 1995;36:1885–1894.
5. Floyd CE, Jaszczak RJ, Greer KL, Coleman RE. Inverse Monte Carlo as an unified reconstruction algorithm for ECT. J Nucl Med 1986;27:1577–1585.
6. Frey EC, Tsui BMW. A practical method for incorporating scatter in a projector-backprojector for accurate scatter compensation in SPECT. IEEE Trans Nucl Sci 1993;40:1107–1116.
7. Beekman FJ, Kamphuis C, Viergever MA. Improved quantitation in SPECT imaging using fully 3D iterative spatially variant scatter compensation. IEEE Trans Med Imaging 1996;15:491–499.
8. Welch A, Gullberg GT, Christian PE, Datz FL. A transmission-map-based scatter correction technique for SPECT in inhomogeneous media. Med Phys 1995;22:1627–1636.
9. Hutton BF, Osiecki A, Meikle SR. Transmission-based scatter correction of 180° myocardial SPECT studies. Eur J Nucl Med 1996;23:1300–1308.
10. Beekman FJ, den Harder JM, Viergever MA, van Rijk PP. SPECT scatter modeling in nonuniform attenuating objects. Phys Med Biol 1997;42:1133–1142.
11. Kamphuis C, Beekman FJ, Viergever MA, van Rijk PP. Dual matrix ordered subset reconstruction for accelerated 3D scatter correction in SPECT. Eur J Nucl Med 1998;25:8–18.
12. King MA, Tsui BMW, Pan TS. Attenuation compensation for cardiac single-photon emission computed tomographic imaging: Part 1, Impact of attenuation and methods of estimating attenuation maps. J Nucl Cardiol 1995;2:513–524.
13. King MA, Tsui BMW, Pan TS, Glick SJ, Soares EJ. Attenuation compensation for cardiac single-photon emission computed tomographic imaging: Part 2, Attenuation compensation algorithms. J Nucl Card 1996;3:55–64.
14. Ogawa K, Takagi Y, Kubo A, et al. An attenuation correction method of SPECT using gamma ray transmission CT. KAKU-IGAKU (Japanese J Nucl Med) 1985;22:477–490.
15. Malko JA, van Heertum RL, Gullberg GT, Kowalsky WP. SPECT liver imaging using an iterative attenuation correction algorithm and an external flood source. J Nucl Med 1986;27:701–705.
16. Bailey DL, Hutton BF, Walker PJ. Improved SPECT using simultaneous emission and transmission tomography. J Nucl Med 1987;28:844–851.
17. Greer KL, Harris CC, Jaszczak RJ, et al. Transmission computed tomography with a SPECT system. J Nucl Med Technol 1987;15:53–56.
18. Tsui BMW, Gullberg G, Edgerton E, et al. Correction of nonuniform attenuation in cardiac SPECT imaging. J Nucl Med 1989;30:497–507.
19. Frey EC, Tsui BMW, Perry JR. Simultaneous acquisition of emission and transmission data for improved thallium-201 cardiac SPECT imaging using a technetium-99m transmission source. J Nucl Med 1992;33:2238–2245.
20. Cao ZJ, Tsui BMW. Performance characteristics of transmission imaging using a nonuniform sheet source with parallel-hole collimation. Med Phys 1992;19:1205–1212.
21. Tan P, Bailey SR, Meikle SR, Eberl S, Fulton RR, Hutton BF. A scanning line source for simultaneous emission and transmission measurements in SPECT. J Nucl Med 1993;34:1752–1759.
22. Turkington T, Wilk M, Wainer N, Coleman RE. Correcting for emission contamination in SPECT scanning line source transmission data [Abstract]. J Nucl Med 1996;37:19P.
23. Jaszczak RJ, Gilland D, Hanson M, Jang S, Greer KL, Coleman R. Fast transmission CT for determining attenuation maps using a collimated line source, rotatable air-copper-lead attenuators and fanbeam collimation. J Nucl Med 1993;34:1577–1586.
24. Tung CH, Gullberg GT. A simulation of emission and transmission noise propagation in cardiac SPECT imaging with nonuniform attenuation correction. Med Phys 1994;21:1565–1576.
25. Kemp BJ, Prato FS, Nicholson RL. The geometric modulation transfer function of a transmission imaging system that uses a SPECT scintillation camera and parallel-hole collimation. Med Phys 1995;22:733–741.

26. Kemp BJ, Prato FS, Nicholson RL, Reese L. Transmission computed tomography imaging of the head with a SPECT system and a collimated line source. *J Nucl Med* 1995;36:328–335.

27. Chang W, Loncaric S, Huang G, Sanpitak P. Asymmetric fan transmission CT on SPECT systems. *Phys Med Biol* 1995;40:913–928.

28. Hawman EG, Ficaro EP, Hamill JJ, Schwaiger M. Fanbeam collimation with off center focus for simultaneous emission/transmission SPECT in multicamera SPECT systems [Abstract]. *J Nucl Med* 1994;35:92.

29. Tsui BMW, Lalush DS, Lewis DP, et al. High-resolution brain SPECT imaging using half fanbeam collimators with a right-angle, dual-camera SPECT system [Abstract]. *J Nucl Med* 1997;38:32P.

30. Tomiguchi S, Kojima A, Oyama Y, et al. Development of asymmetric fanbeam transmission CT on two-head SPECT system [Abstract]. *J Nucl Med* 1997;38:212P.

31. Gilland DR, Jaszczak RJ, Wang H, Coleman RE. Transmission data acquisition with a large-field-of-view dual-head SPECT system [Abstract]. *J Nucl Med* 1997;38:220P.

32. Gilland DR, Wang H, Coleman RE, Jaszczak RJ. Long focal length, asymmetric fanbeam collimation for transmission acquisition with a triple camera SPECT system. *IEEE Trans Nucl Sci* 1997;44:1191–1196.

33. Beekman FJ, Kamphuis C, van Rijk PP. Scanning point sources combined with two half-fanbeam collimators for simultaneous emission and transmission measurements in SPECT [Abstract]. *J Nucl Med* 1997;38:216P.

34. Heller EN, DeMan P, Liu YH, et al. Extracardiac activity complicates quantitative cardiac SPECT imaging using a simultaneous transmission-emission approach. *J Nucl Med* 1997;38:1882–1890.

35. Manglos SH, Bassano DA, Duxbury C, Capone R. Attenuation maps for SPECT determined using cone beam transmission computed tomography. *IEEE Trans Nucl Sci* 1990;37:600–607.

36. Lange K, Fessler JA. Globally convergent algorithms for maximum a posteriori transmission tomography. *IEEE Trans Im Proc* 1995;4:1430–1438.

37. Zeng GL, Hsieh Y, Gullberg GT. A rotating and warping projector-backprojector pair for fanbeam and cone-beam iterative algorithms. *IEEE Trans Nucl Sci* 1994;41:2807–2811.

38. Lange K, Carson REM. Reconstruction algorithms for emission and transmission tomography. *J Comput Assist Tomogr* 1984;8:306–316.

39. Tsui BMW, Zhao XD, Gregouri GK, et al. Quantitative cardiac SPECT reconstruction with reduced image degradation due to patient anatomy. *IEEE Trans Nucl Sci* 1993;41:2838–2844.

40. Jaszczak RJ, Gilland DR, McCormick JW, Scarphone C, Coleman RE. The effect of truncation reduction in fan beam transmission for attenuation correction in cardiac SPECT. *IEEE Trans Nucl Sci* 1996;43:2255–2262.

41. Tung CH, Gullberg GT, Zeng GL, Christian PE, Datz FL, Morgan HT. Nonuniform attenuation correction using simultaneous transmission and emission converging tomography. *IEEE Trans Nucl Sci* 1992;38:1134–1143.

42. King MA, Luo D, Dahlberg S, Penney B, Morgan H. Transmission imaging of large attenuators using a slant hole collimator on a three-head SPECT system. *Med Phys* 1996;23:263–272.

43. Beekman FJ, Kamphuis C. Effects of truncation of transmission projections on cardiac SPECT images acquired by a right-angle dual-camera with half-fanbeam collimators *Conference record of 1997 IEEE nuclear science symposium and medical imaging conference*. Albuquerque, NM: IEEE *Trans Nucl Sci* 1998;45:1174–1178.

44. Luo D, King MA, Morgan HT, et al. Investigations into possible causes of hot inferior wall artifacts in attenuation-corrected cardiac perfusion images. *IEEE Trans Nucl Sci* 1997;44:1146–1153.

45. Floyd CE, Jaszczak RJ, Harris CC, Coleman RE. Energy and spatial distribution of multiple order Compton scatter in SPECT; a Monte Carlo investigation. *Phys Med Biol* 1984;29:1217–1230.

46. Beekman FJ, Viergever MA. Fast SPECT simulation including object shape dependent scatter. *IEEE Trans Med Imaging* 1995;14:271–282.

47. Frey EC, Tsui BMW. A new method for modeling the spatially variant object dependent scatter response function in SPECT. *1996 IEEE nuclear science symposium conference record*. Anaheim, CA: IEEE; November 1996:1082–1086.

48. Kadrmas DJ, Jaszczak RJ, McCormick JW, Coleman RE, Lim CB. Truncation artifact reduction in transmission CT for improved SPECT attenuation compensation. *Phys Med Biol* 1995;40:1085–1104.

49. Zeng GL, Gullberg GT. An SVD study of truncated transmission data in SPECT. *IEEE Trans Nucl Sci* 1997;44:107–111.

Imaging of Adenoviral-Directed Herpes Simplex Virus Type 1 Thymidine Kinase Reporter Gene Expression in Mice with Radiolabeled Ganciclovir

Sanjiv S. Gambhir, Jorge R. Barrio, Lily Wu, Meera Iyer, Mohammad Namavari, Nagichettiar Satyamurthy, Eileen Bauer, Capella Parrish, Duncan C. MacLaren, Ali R. Borghei, Leeta A. Green, Susan Sharfstein, Arnold J. Berk, Simon R. Cherry, Michael E. Phelps and Harvey R. Herschman

Crump Institute for Biological Imaging; UCLA/DOE Laboratory of Structural Biology and Molecular Medicine; Department of Molecular and Medical Pharmacology, Division of Nuclear Medicine; Molecular Biology Institute; Department of Biomathematics; and UCLA-Jonsson Comprehensive Cancer Center, UCLA School of Medicine, Los Angeles, California

We are developing procedures to repeatedly and noninvasively image the expression of transplanted reporter genes in living animals and in patients, using PET. We have investigated the use of the Herpes Simplex Virus type 1 thymidine kinase gene (HSV1-tk) as a reporter gene and [8-^{14}C]-ganciclovir as a reporter probe. HSV1-tk, when expressed, leads to phosphorylation of [8-^{14}C]-ganciclovir. As a result, specific accumulation of phosphorylated [8-^{14}C]-ganciclovir should occur almost exclusively in tissues expressing the HSV1-tk gene. **Methods:** An adenoviral vector was constructed carrying the HSV1-tk gene along with a control vector. C6 rat glioma cells were infected with either viral vector and uptake of [8-^{3}H]-ganciclovir was determined. In addition, 12 mice were injected with varying levels of either viral vector. Adenovirus administration in mice leads primarily to liver infection. Forty-eight hours later the mice were injected with [8-^{14}C]-ganciclovir, and 1 hr later the mice were sacrificed and biodistribution studies performed. Digital whole-body autoradiography also was performed on separate animals. HSV1-tk expression was assayed, using both normalized HSV1-tk mRNA levels and relative HSV1-TK enzyme levels, in both the cell culture and murine studies. **Results:** Cell culture, murine tissue biodistribution and murine in vivo digital whole-body autoradiography all demonstrate the feasibility of HSV1-tk as a reporter gene and [8-^{14}C]-ganciclovir as an imaging reporter probe. A good correlation ($r^2 = 0.86$) between the [8-^{14}C]-ganciclovir percent injected dose per gram tissue from HSV1-tk positive tissues and HSV1-TK enzyme levels in vivo was found. An initial study in mice with [8-^{18}F]-fluoroganciclovir and microPET imaging supports further investigation of [8-^{18}F]-fluoroganciclovir as a PET reporter probe for imaging HSV1-tk gene expression. **Conclusion:** These results demonstrate the feasibility of using [8-^{14}C]-ganciclovir as a reporter probe for the HSV1-tk reporter gene, using an in vivo adenoviral mediated gene delivery system in a murine model. The results form the foundation for further investigation of [8-^{18}F]-fluoroganciclovir for noninvasive and repeated imaging of gene expression with PET.

Key Words: reporter gene; imaging; PET; thymidine kinase; gene expression